

Electron-phonon coupling in ferromagnetic Fe-Co alloys from first principles

Kevin Moseni,^{1,*} Richard B. Wilson,^{1,2} and Sinisa Coh^{1,2}

¹*Materials Science and Engineering, University of California Riverside, Riverside, CA 92521, USA*

²*Mechanical Engineering, University of California Riverside, Riverside, CA 92521, USA*

We calculate from first principles the electron-phonon coupling strength in ferromagnetic iron-cobalt $\text{Fe}_{1-x}\text{Co}_x$ alloys for compositions ranging from $x = 0$ to $x = 0.75$. We find strong, spin-dependent variation of the electron-phonon coupling strength with alloy composition. The minimum of the electron-phonon interaction is found near the composition $x = 0.25$. We analyze the variation of the electron-phonon interaction with composition, as a function of electron spin, density of states, electron-phonon matrix elements, and phonon frequencies. Our results are in good qualitative agreement with magnetization dynamics experiments.

I. INTRODUCTION

Electron-phonon coupling plays a key role in understanding the dynamic properties of magnets, including Gilbert damping,[1] ultrafast demagnetization,[2] all-optical switching,[3] and spin-dependent transport.[4, 5] Engineering these magnetic properties requires an understanding of the material parameters, like electron density of states or electron-phonon matrix elements, that affect the strength of electron-phonon coupling. Until recently, studies of electron-phonon coupling strength in magnets have focused on only a small subset of ferromagnetic materials, namely the elemental ferromagnets Ni, Fe, and Co. However, many ferromagnets are alloys of transition metals. One such example is the Fe-Co alloy. Magnetic damping in the Fe-Co alloy was only recently measured.[6] Interestingly, Ref. 6 reports significant changes in damping as a function of the Fe-Co alloy composition. In particular, the lowest damping was measured in the $\text{Fe}_{0.75}\text{Co}_{0.25}$ alloy, the same alloy composition that the density of states is lowest. Measurements of the minimal damping in this composition has been reported by others.[7, 8] More recent experiments showed that the demagnetization response is maximized in this composition due to a minimum in the electron-phonon energy transfer coefficient,[9] a quantity that depends not only on the density of states but also the electron-phonon matrix elements.

Our goal in this work is to understand the composition dependence of the electron-phonon coupling strength in the ferromagnetic Fe-Co alloy. As we detail in Sec. II, surprisingly few computational first-principles studies of the electron-phonon coupling strength in ferromagnetic alloys exist, aside from the study of electron-phonon energy transfer coefficient in Ni-based alloys.[10] Although λ has been reported for pure Fe and Co, [11] no results have been reported for λ in Fe-Co alloys. On the other hand, similar studies exist for many non-magnetic alloys as a function of their composition. The electron-phonon coupling strength in some alloys, such as V-Cr, varies linearly with composition,[12] as one might expect from a

rule of mixtures. But in other cases, such as Nb-Mo, there is non-linear dependence of the electron-phonon coupling strength on the composition.[13]

In this work we use first principles density functional theory to compute the electron-phonon coupling strength λ in Fe-Co alloys. We find that λ varies strongly, and non-monotonically, with alloy composition, reaching a minimum near the aforementioned $\text{Fe}_{0.75}\text{Co}_{0.25}$ composition. We perform a spin decomposition of λ and find that the majority-spin contribution to λ monotonically decreases with the alloy composition, while the opposite is true for minority-spin. We further analyze the quantities driving the composition dependence of λ and we find that while the density of states plays a dominant role, the magnitude of the electron-phonon matrix elements also varies strongly with the alloy composition. We compare our theoretical results with experimental estimates of the electron-phonon energy transfer coefficient in Fe-Co alloys across a range of compositions [9] and find that our results are qualitatively in agreement with the experiment.

The structure of this paper is as follows. In Sec. II, we discuss previous experimental and theoretical values of the electron-phonon coupling strength in metallic alloys. In Sec. III, we detail how we decompose the electron-phonon interaction strength into their spin components. Then in Sec. IV, we show the results of the first-principles density functional theory for the electron-phonon coupling strength in ferromagnetic Fe-Co alloys. We analyze separately the strengths of majority- and minority-spin components in order to reveal the origin of the nonmonotonicity. We also compare our results with experiments. In Sec. V, we conclude.

II. ELECTRON PHONON COUPLING IN ALLOYS

The dependence of λ on alloy composition has been studied for various nonmagnetic alloy systems. These include empirical values of λ , estimated from the ratio of the Debye temperature and the superconducting transition temperature, in ordered and disordered alloys,[12, 14] as well as first principles calculated λ

* kevinmoseni@gmail.com

in virtual crystal approximated alloys[15–17], ordered alloys,[18] and disordered alloys.[19, 20] Naively, one might think that λ in an alloy $A_{1-x}B_x$ with composition x could be calculated by linear interpolation from the electron-phonon coupling strength of metal A (λ_A) to that of metal B (λ_B). To evaluate how well the linear model approximates λ , we computed

$$\lambda^{\text{linear}} = (1-x)\lambda_A + x\lambda_B \quad (1)$$

for the various alloys in the literature. For many of the alloys, the literature contains values for λ for only part of the range of compositions. For these, we linearly interpolate from λ at the lowest available composition x_{min} to λ at the highest available composition x_{max} using a simple generalization of Eq. 1,

$$\lambda^{\text{linear}} = \frac{x_{\text{max}} - x}{x_{\text{max}} - x_{\text{min}}} \lambda_{x_{\text{min}}} + \frac{x - x_{\text{min}}}{x_{\text{max}} - x_{\text{min}}} \lambda_{x_{\text{max}}}. \quad (2)$$

However, as expected, this naive linear approximation is valid only for a few alloys. The deviations from the linear behavior are quite commonly reported in the literature,[12–14, 16–22] as summarized in Fig. 1. The vertical axis in Fig. 1 shows λ and the horizontal scale of the figure shows the composition ranging from x_{min} to x_{max} for each alloy based on the available data.

We further quantify the deviation from the naive linear model by computing $\frac{\lambda - \lambda^{\text{linear}}}{\lambda^{\text{linear}}} \times 100$ for each alloy, as shown in Fig. 2.

As can be seen from Fig. 2, the $V_{1-x}Cr_x$ alloy in the range of $x = 0.1$ to $x = 0.5$ has a reported relative deviation from the naive linear estimation of only -1%. On the other hand, in Ti-V and Mo-Re alloys, the deviation from linear dependence is up to 20%, while in the Pb-Tl, VN-NbN, Nb-Mo, and Ta-W alloys it is even greater, around $\pm 40\%$. The largest deviation from the linear regime, about 80%, was found for ordered $Cu_{3/4}Au_{1/4}$ alloy. We note that the linear dependence of λ on composition in some alloy systems (Zr-Rh, Ag-Zn, Pb-Bi, and Ag-Al) is due to a relatively narrow reported range of composition (x).

Our results on the ferromagnetic Fe-Co alloy are shown in the bottom left panels of Fig. 1 and Fig. 2 in black. We find that λ of $Fe_{0.25}Co_{0.75}$ is about 70% smaller than that predicted by the naive linear model, λ^{linear} .

We now turn our attention to the definitions of key quantities that we will use to study the electron-phonon coupling in Fe-Co alloys.

III. METHODS

The strength of electron-phonon coupling is often measured by a single dimensionless number, λ . [12, 23] The coupling constant λ is defined as a double sum over the

Fermi surface,

$$\lambda = \frac{1}{N_F} \frac{1}{N_k N_q} \sum_{q\nu} \frac{1}{\hbar\omega_{q\nu}} \sum_{mn,k} |g_{mn\nu}(k, q)|^2 \times \delta(\epsilon_{nk} - \epsilon_F) \delta(\epsilon_{mk+q} - \epsilon_F). \quad (3)$$

We denote the total density of states at the Fermi level, for both spin channels, as N_F , the number of sampled k -points in the electron Brillouin zone as N_k , and number of sampled q -points in the phonon Brillouin zone as N_q . The phonon frequency is $\omega_{q\nu}$. The first sum in Eq. 3 goes over phonon q points and branches ν , while the second sum goes over k points and electronic bands m and n . For now, spin indices are incorporated into the band indices. The energy conservation is maintained by the two delta functions. The electron-phonon matrix element $g_{mn\nu}(k, q)$ from Eq. 3 is defined as

$$g_{mn\nu}(k, q) = \sqrt{\frac{\hbar}{2m\omega_{q\nu}}} \langle \psi_{mk+q} | \partial_{q\nu} v | \psi_{nk} \rangle. \quad (4)$$

Here, $\partial_{q\nu} v$ is the periodic modulation of the crystal potential v due to phonon (q, ν) that allows an electron in the state (n, k) to scatter to state $(m, k+q)$.

A. Spin-resolved measures of electron-phonon interaction

For materials with a small spin-orbit interaction, the electronic states have a well-defined spin. Therefore, from now on we use $\sigma = \uparrow$ or $\sigma = \downarrow$ to index the Bloch state ψ_{nk}^σ with a specific spin state. In the small spin-orbit limit the dominant scattering is between states of equal spin,

$$g_{mn\nu}^\sigma(k, q) = \sqrt{\frac{\hbar}{2m\omega_{q\nu}}} \langle \psi_{mk+q}^\sigma | \partial_{q\nu} v | \psi_{nk}^\sigma \rangle. \quad (5)$$

Under this assumption, the sums over m and n in Eq. 3 trivially decompose into two separate sums, one where both bra and ket states have $\sigma = \uparrow$ and another where both states have $\sigma = \downarrow$ component.

With this separation, λ from Eq. 3 decomposes into two terms, one for each spin channel σ ,

$$\lambda = \lambda^\uparrow + \lambda^\downarrow. \quad (6)$$

The spin-dependent quantity λ^σ is defined as

$$\lambda^\sigma = \frac{1}{N_F^\uparrow + N_F^\downarrow} \frac{1}{N_k N_q} \sum_{q\nu} \frac{1}{\hbar\omega_{q\nu}} \sum_{mn,k} |g_{mn\nu}^\sigma(k, q)|^2 \times \delta(\epsilon_{nk}^\sigma - \epsilon_F) \delta(\epsilon_{mk+q}^\sigma - \epsilon_F). \quad (7)$$

The only difference between total λ from Eq. 3 and spin-resolved λ^σ from Eq. 7 is that the former involves a sum over all states, while the latter sums over states with

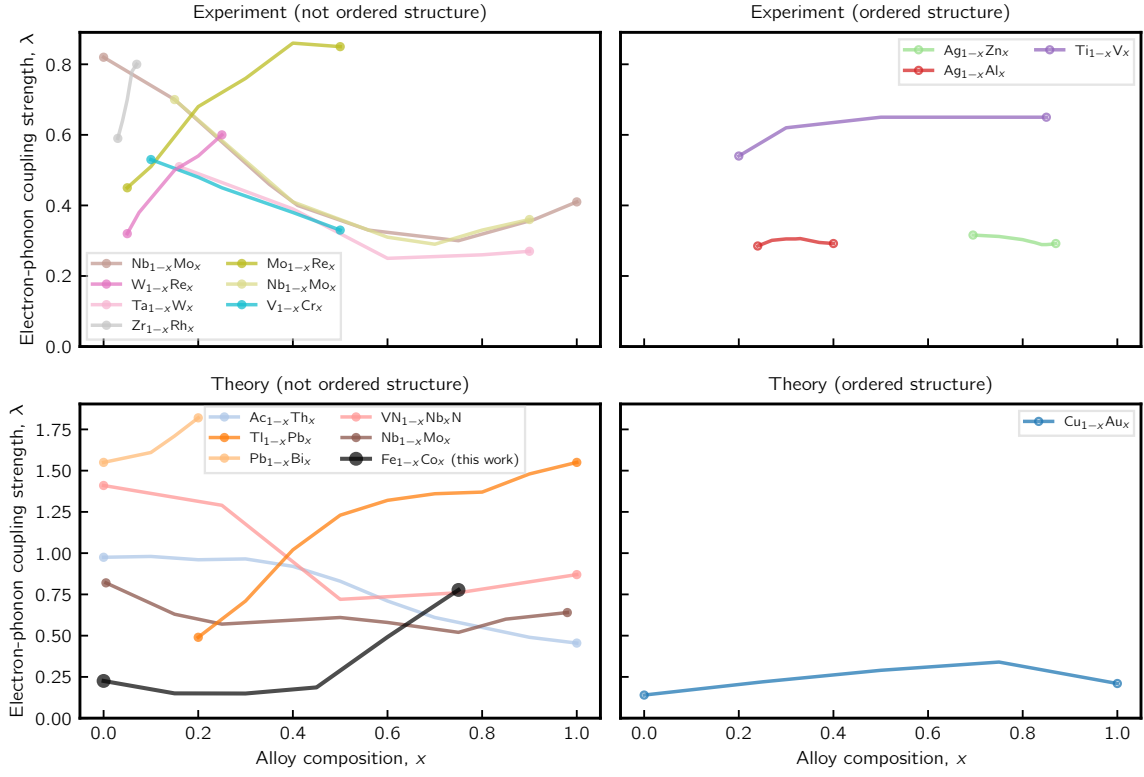


FIG. 1. Dependence of the electron-phonon coupling strength (λ) on composition (x). Experimental results are from Refs. 12, 13, 21, and 22. Theoretical results are from Refs. 16–20.

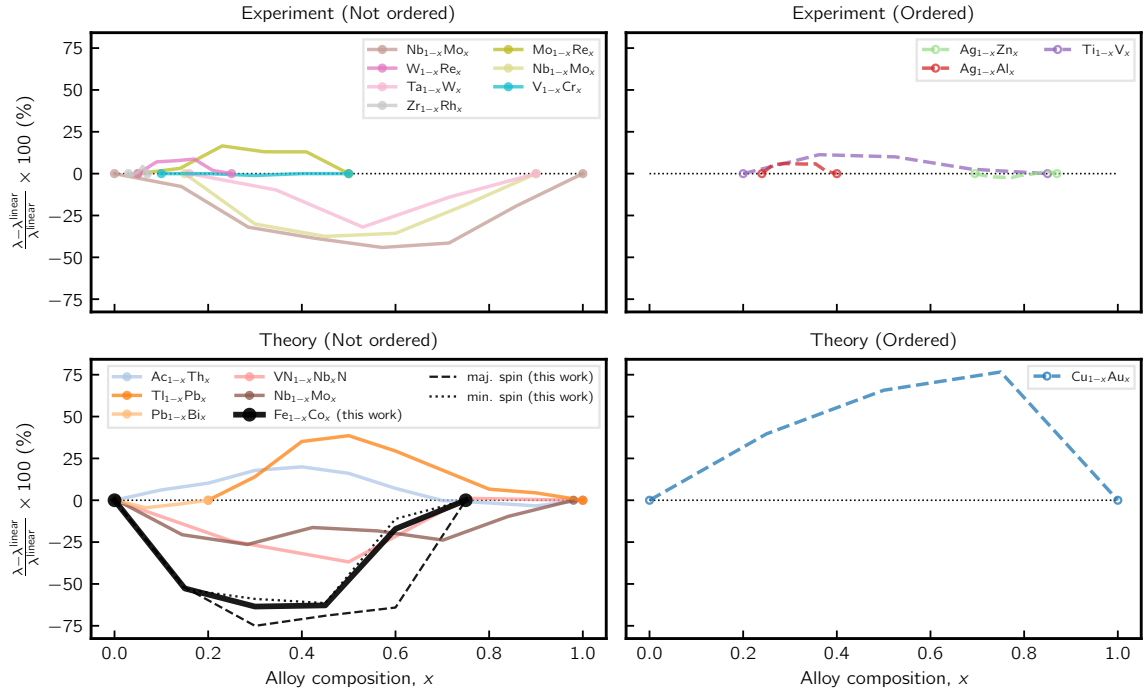


FIG. 2. Same as Fig. 1 but now instead of λ we show deviation of λ from the linear model given by Eq. 2.

fixed spin σ . Importantly, in Eq. 7 of the spin-resolved quantity λ^σ we still have the total density of states $N_F = N_F^\uparrow + N_F^\downarrow$ in the denominator.

In what follows it will be convenient to work with the Eliashberg spectral function, $\alpha^2 F(\omega)$, as it keeps track of the phonon frequencies ω which connect the electron states with wavevector k to a state with the wavevector $k + q$, both of which are at or near the Fermi surface.[12, 24] We denote the wavevector of a phonon with q . In analogy to the decomposition of λ into two spin components, we decompose the Eliashberg spectral function into contributions from each spin channel, $\alpha^2 F^\sigma(\omega)$. We define this spin-resolved quantity so that integrating over $d\omega/\omega$ gives back our additive spin-resolved λ^σ ,

$$\lambda^\sigma = 2 \int_0^\infty \frac{d\omega}{\omega} \alpha^2 F^\sigma(\omega). \quad (8)$$

Therefore, clearly, in analogy to Eq. 6 we have

$$\alpha^2 F(\omega) = \alpha^2 F^\uparrow(\omega) + \alpha^2 F^\downarrow(\omega) \quad (9)$$

where $\alpha^2 F(\omega)$ is the conventional Eliashberg spectral function used, for example, in the study of superconductivity and elsewhere.

1. Alternative definition: non-additive λ

Previous work on electron-phonon coupling in ferromagnetic metals, Ref. 11, introduced a different measure of spin-resolved electron-phonon coupling strength. Instead of dividing by the total density of states, as in Eq. 7, we divide by a spin-resolved density of states. This leads to a quantity $\lambda_{\text{nadd}}^\sigma$ which is related to λ^σ simply as,

$$\lambda_{\text{nadd}}^\sigma = \frac{N_F^\uparrow + N_F^\downarrow}{N_F^\sigma} \lambda^\sigma. \quad (10)$$

Clearly, such $\lambda_{\text{nadd}}^\sigma$ is no longer additive over spins. Instead, using Eqs. 6 and 10 we have the following relation,

$$\lambda = \frac{N_F^\uparrow \lambda_{\text{nadd}}^\uparrow + N_F^\downarrow \lambda_{\text{nadd}}^\downarrow}{N_F^\uparrow + N_F^\downarrow}. \quad (11)$$

While definition of $\lambda_{\text{nadd}}^\sigma$ somewhat complicates its relation to the total λ , a common measure of electron-phonon interaction in the literature, the quantity $\lambda_{\text{nadd}}^\sigma$ has another convenient property. If we for a moment neglect some of the details of the electronic band structure, and assume that the electron-phonon matrix elements on the Fermi surface are independent of band indices m, n , then the matrix element can be taken out of the double sum, and the sum over the two delta functions gives us $(N_F^\sigma)^2$ which partially cancels N_F^σ from the denominator. Therefore, relationship between non-additive $\lambda_{\text{nadd}}^\sigma$ and the average electron-phonon matrix element $\langle g_\sigma^2 \rangle$ for a given spin-channel is particularly straightforward,

$$\lambda_{\text{nadd}}^\sigma = N_F^\sigma \langle g_\sigma^2 \rangle. \quad (12)$$

On the other hand, if one wanted to relate our additive λ^σ to the average matrix element, combining Eqs. 10 and 12 would lead to a less intuitive relationship with the average matrix element strength,

$$\lambda^\sigma = \frac{(N_F^\sigma)^2}{N_F^\uparrow + N_F^\downarrow} \langle g_\sigma^2 \rangle. \quad (13)$$

B. Relationship to electron-phonon energy transfer coefficient G

Now we relate our λ and λ^σ to the electron-phonon energy transfer coefficient G . This coefficient describes the rate of energy transfer between electrons and phonons per unit volume and per temperature difference of electrons and phonons. Within the two-temperature model of electrons and phonons for a nonmagnetic system,[25] G is proportional to the total density of states $N_F = N_F^\uparrow + N_F^\downarrow$ and λ . This model implicitly assumes that majority and minority spins are thermalized with each other at all times. With this assumption, the effective G for a spin-polarized system is given as,

$$G = \frac{\pi k_B \hbar}{V_c} \left[(N_F^\uparrow + N_F^\downarrow) (\lambda^\uparrow + \lambda^\downarrow) \right] \langle \omega^2 \rangle \quad (14)$$

using additive λ^σ , or equivalently

$$G = \frac{\pi k_B \hbar}{V_c} \left(N_F^\uparrow \lambda_{\text{nadd}}^\uparrow + N_F^\downarrow \lambda_{\text{nadd}}^\downarrow \right) \langle \omega^2 \rangle \quad (15)$$

using the non-additive variant. Here V_c is the unit cell volume (per atom), and $\langle \omega^2 \rangle$ is a weighted average of the square of the phonon frequency, defined as[12]

$$\langle \omega^2 \rangle = \frac{2}{\lambda^\uparrow + \lambda^\downarrow} \int_0^\infty d\omega \omega \left[\alpha^2 F^\uparrow(\omega) + \alpha^2 F^\downarrow(\omega) \right], \quad (16)$$

with units of meV^2 . Equations 14 and 15 give a numerically equal energy transfer coefficient G . Therefore, additive λ^σ or non-additive $\lambda_{\text{nadd}}^\sigma$ can be used to compute G . The only difference between the two equations is that they implicitly assume a different thermodynamic description of the electronic system. In the case of Eq. 14 one considers the electronic system in a ferromagnet as one unified thermal reservoir. The effective electron-phonon coupling strength for this system is then the sum of λ^\uparrow and λ^\downarrow . In contrast, in the case of Eq. 15, one imagines the electronic system as consisting of two reservoirs, one for each spin, and each subsystem has its density of states and effective electron-phonon coupling strength.

As with λ , we can separate G into its majority-spin part G^\uparrow and minority-spin part G^\downarrow ,

$$G = G^\uparrow + G^\downarrow \quad (17)$$

where the electron-phonon energy transfer coefficient for spin channel σ is defined as

$$G^\sigma = \frac{\pi k_B \hbar}{V_c} (N_F^\uparrow + N_F^\downarrow) 2 \int_0^\infty d\omega \omega \alpha^2 F^\sigma(\omega). \quad (18)$$

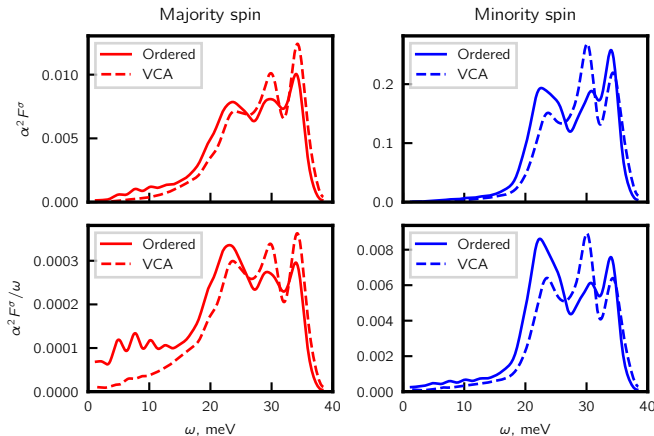


FIG. 3. $\alpha^2 F^\sigma$ and $\alpha^2 F^\sigma / \omega$ for FeCo alloy calculated for an ordered supercell (solid lines) and within the VCA (dashed lines) for majority spins (left column) and minority spins (right column).

C. Details of density functional theory calculation

In this work, we used the QUANTUM ESPRESSO computer package[26, 27] for density functional theory calculations. We selected non-relativistic ONCV pseudopotentials [28] for Fe and Co. We used 90 Ry kinetic-energy cutoff and 18^3 k points on a uniform grid to converge wavefunctions. We used the density functional perturbation theory to calculate the phonons on a coarse grid of 4^3 q points. We constructed Wannier functions using Wannier90,[29–31] and we computed the electron-phonon matrix elements with EPW.[32, 33] The convergence of λ^σ requires a small smearing parameter and a large number of k -points and q -points. We vary these parameters until convergence in the limit of zero smearing and infinitely many k and q points. We determined that 72^3 k points and 24^3 q points is sufficient to converge λ^σ . To converge the density of states at the Fermi energy, we used 192^3 k points. We modified the native EPW package to support spin-polarized calculations. All of our calculations are done without including the spin-orbit interaction, as it is relatively weak in $3d$ metals such as Fe and Co.

D. Virtual-crystal approximation

In this work, we focus on $\text{Fe}_{1-x}\text{Co}_x$ alloys in the range of concentrations $0 < x < 0.75$. Pure iron ($x = 0$) at room temperature adopts a body-centered cubic structure (bcc, space group $Im\bar{3}m$). When Co is added to Fe, the structure remains bcc, but Fe and Co atoms are randomly arranged on a bcc lattice. At a higher concentration of Co ($x = 0.5$) there is an ordering of Fe and Co atoms (B_2 phase, space group $Pm\bar{3}m$).[34, 35] At an even higher concentration of Co (above around $x = 0.75$) the

bcc phase is no longer favored and the preferred phase is hexagonal close-packed (hcp). Therefore, we choose to study the range of concentrations at which the alloy is single phased and assume that the structure of the alloy is bcc or ordered B_2 , depending on the concentration.

We model $\text{Fe}_{1-x}\text{Co}_x$ alloys within the virtual crystal approximation (VCA).[36] Briefly, we use two elemental pseudopotentials and combine them with the desired fraction of each element to create an effective pseudopotential of the alloy. Then we place the pseudopotential of the alloy in the primitive cell of the bcc lattice (2a site of space group $Im\bar{3}m$) to generate the bcc alloy. The VCA approach offers a computational advantage, because we can use a single atom basis to represent arbitrary alloy compositions x , eliminating the need for computationally expensive supercell calculations. To compare our results to that of a supercell, we computed λ at $x = 0.5$ using both approaches. To construct the supercell, we place Fe in the 1a site and Co in the 1b site of the space group $Pm\bar{3}m$, resulting in an ordered (B_2) $\text{Fe}_{1/2}\text{Co}_{1/2}$ alloy.

On converging both calculations we find that in the ordered $\text{Fe}_{1/2}\text{Co}_{1/2}$ alloy, λ is 0.496 while in the VCA approach λ is surprisingly similar, 0.491. We find a similar agreement in λ^\uparrow and λ^\downarrow . To further compare these calculations, we first recall that λ^σ is the product of $\frac{(N_F^\sigma)^2}{N_F^\uparrow + N_F^\downarrow}$ and the average matrix element $\langle g_\sigma^2 \rangle$. Comparing the values obtained from both methods, we find that the VCA overestimates $\frac{(N_F^\uparrow)^2}{N_F^\uparrow + N_F^\downarrow}$ by 20%, and underestimates $\langle g_\uparrow^2 \rangle$ by 10%. The opposite is true for the minority spins: underestimation of $\frac{(N_F^\downarrow)^2}{N_F^\uparrow + N_F^\downarrow}$ and overestimation of $\langle g_\downarrow^2 \rangle$. Therefore, the remarkably close agreement in λ^σ and λ obtained from VCA and supercell is partly due to accidental partial cancellation of errors in the densities of states and electron-phonon matrix elements. To further analyze our results, we compare the spin-resolved Eliashberg spectral functions (shown in Fig. 3) and we find that the supercell approach gives a spectral function that has more features, especially at low frequencies. Furthermore, we find some weight redistribution among the peaks at higher part of the phonon spectrum. We assign these differences to the folding of the band structure in the supercell approach that is absent in the VCA. Given the large number of k and q points needed to converge these calculations, the numerically precise calculation of λ for other values of x quickly becomes computationally prohibitive.

IV. RESULTS & DISCUSSION

Now we discuss the results of our calculations of λ in $\text{Fe}_{1-x}\text{Co}_x$ for x between 0 and 0.75 in steps 0.125. In the case of pure Fe ($x = 0$), we find λ to be 0.23. As we increase the Co concentration x , we find that λ first decreases for small x and then increases substantially for larger x , as shown by the black line in Figure 4. The

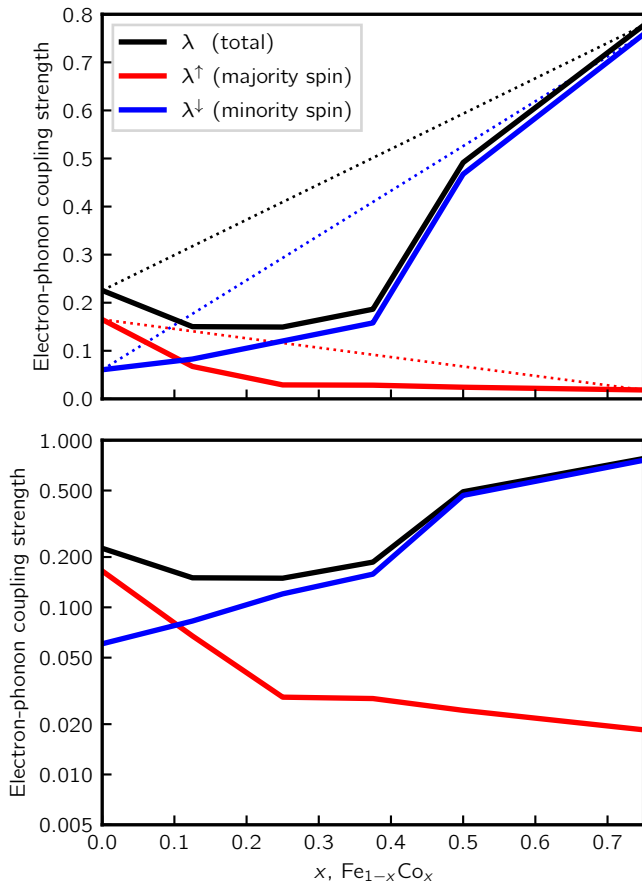


FIG. 4. Electron-phonon coupling strength λ (black line) is a nonmonotonic function of the alloy composition x . The majority-spin λ^\uparrow (red line) decreases with composition as the minority-spin λ^\downarrow (blue line) increases. The top panel has a linear vertical scale, and the bottom panel has a logarithmic vertical scale. The results shown here are from VCA.

numerical values of λ are also shown in Table I. Between concentrations $x = 0$ and $x = 0.125$, λ decreases by a factor of 1.5. As the concentration increases further, we find that λ increases by a factor of 5 between $x = 0.25$ and $x = 0.75$. Table I also contains numerical values of the electron-phonon energy transfer coefficient G calculated using Eqs. 14 and 16.

A. Resolving λ into electron spin

To understand the origin of the initial decrease followed by a sudden increase in λ as a function of x , we use our decomposition of λ into the majority-spin part λ^\uparrow and the minority-spin part λ^\downarrow , as defined in Sec III. We show in Fig. 4 the λ^\uparrow (red line) and λ^\downarrow (blue line) as a function of the alloy composition x . We also show the numerical values in Table I. The majority spin λ^\uparrow is dominant over the minority spin λ^\downarrow in pure Fe ($x = 0$). However, the previously dominant λ^\uparrow drastically reduces

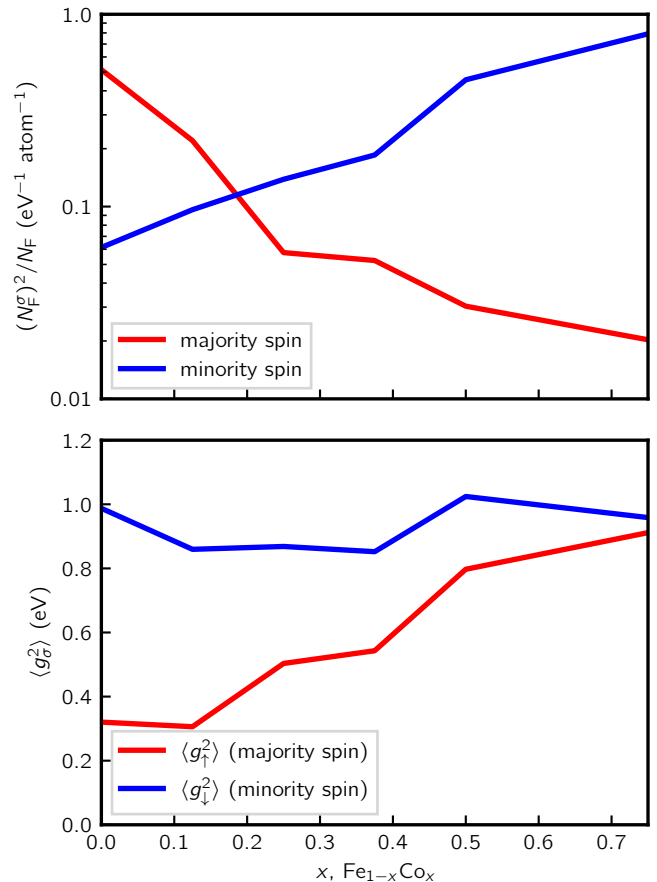


FIG. 5. Compositional dependence of $\frac{(N_F^g)^2}{N_F^\uparrow + N_F^\downarrow}$ (top panel, log scale) and average electron-phonon matrix element $\langle g_\sigma^2 \rangle$ (bottom panel, linear scale). With increasing x the majority spin $\frac{(N_F^\uparrow)^2}{N_F^\uparrow + N_F^\downarrow}$ decreases, while the minority spin $\frac{(N_F^\downarrow)^2}{N_F^\uparrow + N_F^\downarrow}$ increases. The average matrix element of the majority spins $\langle g_\uparrow^2 \rangle$ increases with x while the minority spin $\langle g_\downarrow^2 \rangle$ is constant.

in magnitude between $x = 0$ and $x = 0.25$, and remains small (around 0.02) until $x = 0.75$. The minority λ^\downarrow has the opposite behavior. Although λ^\downarrow was small in Fe ($x = 0$) it increases about 12-fold as concentration x of Co increases from $x = 0$ to $x = 0.75$. The cross-over from $\lambda^\uparrow > \lambda^\downarrow$ to $\lambda^\uparrow < \lambda^\downarrow$ occurs already around $x = 0.125$.

Therefore, the dependence of λ on x in $\text{Fe}_{1-x}\text{Co}_x$ is due to the different behavior of the majority-spin and minority-spin channels. This behavior is in a clear contrast to the nonmagnetic alloys discussed in Sec. II, where by definition $\lambda^\uparrow = \lambda^\downarrow$. Therefore, trivially, any nonlinearity in $\lambda(x)$ for a nonmagnetic alloy cannot come from the different dependence of $\lambda^\uparrow(x)$ compared to $\lambda^\downarrow(x)$.

TABLE I. Quantities related to the electron-phonon coupling in the $\text{Fe}_{1-x}\text{Co}_x$ alloys. N_{F}^{σ} , N_{F} in units of $\text{eV}^{-1}\text{atom}^{-1}$, $\langle g_{\sigma}^2 \rangle$ in units of eV, G in units of $10^{17} \text{Wm}^{-3}\text{K}^{-1}$, magnetic moment μ in units of μ_B/atom , and cell volume (per atom) V_c in units of \AA^3 . The theoretical results from Refs. 11, 37–41 and experimental result from Ref. 42 are included for comparison.

		Fe ($x = 0$)	$x = 0.125$	$x = 0.25$	$x = 0.375$	$x = 0.5$		$x = 0.75$
		Ordered	VCA	VCA	VCA	VCA	Ordered	VCA
N_{F}^{\uparrow}	This work	0.693	0.366	0.147	0.151	0.148	0.145	0.147
	Ref. 11	0.519						
	Ref. 39	0.76		0.12		0.12		
	Ref. 40	0.70						
$N_{\text{F}}^{\downarrow}$	This work	0.239	0.242	0.228	0.284	0.574	0.634	0.918
	Ref. 11	0.312						
	Ref. 39	0.24		0.28		0.58		
	Ref. 40	0.27						
N_{F}	This work	0.932	0.608	0.375	0.435	0.722	0.779	1.065
	Ref. 11	0.831						
	Ref. 39	1.00		0.40		0.70		
	Ref. 40	0.970						
$\langle g_{\uparrow}^2 \rangle$	This work	0.320	0.306	0.503	0.543	0.797	0.966	0.912
	Ref. 11	0.131 ^a						
$\langle g_{\downarrow}^2 \rangle$	This work	0.987	0.860	0.868	0.852	1.024	0.912	0.959
	Ref. 11	0.561 ^a						
$\lambda_{\text{nadd}}^{\uparrow}$	This work	0.222	0.112	0.074	0.082	0.118	0.140	0.134
	Ref. 11	0.068						
$\lambda_{\text{nadd}}^{\downarrow}$	This work	0.236	0.208	0.198	0.242	0.588	0.578	0.88
	Ref. 11	0.175						
λ^{\uparrow}	This work	0.165	0.067	0.029	0.028	0.024	0.026	0.018
	Ref. 11	0.042 ^b						
λ^{\downarrow}	This work	0.061	0.083	0.120	0.158	0.467	0.470	0.759
	Ref. 11	0.066 ^b						
λ	This work	0.226	0.150	0.149	0.186	0.491	0.496	0.777
	Ref. 11	0.108 ^c						
G^{\uparrow}	This work	4.76	1.69	0.499	0.551	0.792	0.637	0.641
G^{\downarrow}	This work	2.49	2.34	2.19	3.46	15.1	14.8	27.2
G	This work	7.25	4.03	2.68	4.01	15.9	15.5	27.9
	Ref. 41	7.00						
	Ref. 37	20.8						
	Ref. 38	10.5						
	Ref. 42	8.80 ^d						
	Ref. 42	9.40 ^e						
μ	This work	2.25	2.37	2.34	2.35	2.23	2.28	2.01
V_c	This work	11.50	11.57	11.53	11.49	11.42	23.16	11.27

^a Calculated by inserting $\lambda_{\text{nadd}}^{\sigma}$ and N_{F}^{σ} from Ref. 11 into our Eq. 12.

^b Calculated by inserting $\lambda_{\text{nadd}}^{\sigma}$ and N_{F}^{σ} from Ref. 11 into our Eq. 10.

^c Calculated by inserting $\lambda_{\text{nadd}}^{\sigma}$ and N_{F}^{σ} from Ref. 11 into our Eq. 11.

^d Direct heating of the sample, as discussed in Ref. 42.

^e Indirect heating of the sample, as discussed in Ref. 42

B. Resolving λ into electronic density of states and electron-phonon matrix elements

Next, we discuss the origin of the composition dependence of λ^\uparrow and λ^\downarrow . We use Eq. 13 to decompose λ^σ into a product of $\frac{(N_F^\sigma)^2}{N_F^\uparrow + N_F^\downarrow}$ and $\langle g_\sigma^2 \rangle$. We begin with an analysis of the composition dependence of the spin-resolved quantity $\frac{(N_F^\sigma)^2}{N_F^\uparrow + N_F^\downarrow}$, as shown in the top panel of Fig. 5 (for N_F^σ and $N_F^\uparrow + N_F^\downarrow$, see Table I). We observe that $\frac{(N_F^\sigma)^2}{N_F^\uparrow + N_F^\downarrow}$ qualitatively tracks the dependence of λ^σ on composition (x). That is, at small x the $\frac{(N_F^\uparrow)^2}{N_F^\uparrow + N_F^\downarrow}$ is larger than $\frac{(N_F^\downarrow)^2}{N_F^\uparrow + N_F^\downarrow}$ but with increasing x they switch. Clearly, a large part of the dependence of λ^σ on the composition (x) comes from the density of states. However, the matrix elements also play a role in the dependence of λ^\uparrow on x . The bottom panel of Fig. 5 shows the majority $\langle g_\uparrow^2 \rangle$ (red line) and the minority $\langle g_\downarrow^2 \rangle$ (blue line) as a function of x . The same data are also included in Table I. As can be seen in the figure and the table, the average electron-phonon matrix elements depend on the Co concentration, x . We find that $\langle g_\uparrow^2 \rangle$ increases by nearly a factor of 3 from $x = 0$ to $x = 0.75$. Despite the increase in $\langle g_\uparrow^2 \rangle$, the 25-fold decrease in $\frac{(N_F^\uparrow)^2}{N_F^\uparrow + N_F^\downarrow}$ from $x = 0$ to $x = 0.75$ drives the reduction in λ^\uparrow with x . On the other hand, the minority spin $\langle g_\downarrow^2 \rangle$ is roughly constant with x , the difference between the largest and smallest $\langle g_\uparrow^2 \rangle$ is around 20%. We also note that for all x the minority spin $\langle g_\downarrow^2 \rangle$ is larger than the majority spin $\langle g_\uparrow^2 \rangle$. In previous studies of transition metals, the electron-phonon matrix elements with larger magnitudes were associated with states with particular orbital character. For example, Ref. 43 reports that the matrix elements for the scattering involving sp states have larger magnitude than those involving d states in Ag. On the other hand, 44 reports the opposite for Cu, Ag, and Au. However, 45 reports no relationship between the matrix element magnitude and the orbital character.

We now comment on the relationship between the average orbital character of states at the Fermi level and the magnitude of the matrix elements. We start by projecting the Bloch states in each band n and for each wavevector k into Wannier function for a given spin channel with approximate s , p , or d orbital characters. Then we analyze the relative fraction of sp to d states at the Fermi level for both majority-spin and minority-spin channels. We show the results in Fig. 6. Our decomposition shows that in Fe ($x = 0$) the majority spins have a d -like character and as x increases to 0.25 the character changes to equal parts d and sp . Then for x above $x = 0.25$ the majority spins maintain their orbital character. This is not clearly correlated with $\langle g_\uparrow^2 \rangle$, which increases continuously with x . Therefore, we observe no simple relationship between the orbital character of the Fermi surface and the $\langle g_\uparrow^2 \rangle$. However, the minority-spin orbital character is d -

like for all x , and the $\langle g_\uparrow^2 \rangle$ is roughly constant with x . We leave a more detailed analysis for future work.

C. Resolving λ by phonon frequency

After resolving λ into various electronic contributions, we now focus on resolving λ by phonon frequencies. First, we analyze the phonon density of states $F(\omega)$, shown in the top row of Fig. 7. We see that the phonon density of states is roughly unchanging with composition, as expected from the similar masses and interatomic force constants of Fe and Co. To analyze which phonons contribute to λ we computed the Eliashberg spectral function $\alpha^2 F(\omega)$, as defined in Eq. 8. The $\alpha^2 F(\omega)$ keeps track of the phonon frequencies ω with a dominant contribution to λ . The black line in the middle row of Fig. 7 shows $\alpha^2 F(\omega)$ for different alloy compositions, x .

In general, we find, as expected, that $\alpha^2 F$ strongly varies with x , mirroring the strong variation discussed earlier for the integrated quantity, λ . Focusing on pure Fe ($x = 0$) we see that $\alpha^2 F(\omega)$ has two peaks, one near 22 meV and another around 37 meV. A third peak, around 30 meV appears for x above 0.375. The relative strength of the peaks changes as a function of x . For example, at $x = 0$ the dominant peak is the low-frequency one, while above $x = 0.375$ the mid-frequency peak dominates, signaling a different electron-phonon scattering channels for x above 0.375. Figure 7 also shows the decomposition of $\alpha^2 F$ into majority spin $\alpha^2 F^\uparrow$ (shown in red) and minority spin $\alpha^2 F^\downarrow$ (shown in blue). From the spin-decomposition, we see that the origin of the low-frequency peak around 22 meV in pure Fe is from the majority-spin channel. On the other hand, the appearance of the mid-frequency contribution above $x = 0.375$ is mainly due to the minority spin channel.

D. Comparison with previous works

We now compare our results with the literature results. λ in bcc iron was empirically estimated[46] to be 0.9. Later calculations within the rigid muffin-tin approximation found λ ranging around 0.5–0.9.[47, 48]

A more recent Ref. 11 reports density functional theory calculations of the electron-phonon coupling strength in pure Fe. The definition of electron-phonon coupling strength from Ref. 11 is equivalent to our non-additive $\lambda_{\text{nadd}}^\sigma$ from Eq. 10. The reported values of the non-additive $\lambda_{\text{nadd}}^\sigma$ are 0.068 for majority spins and 0.175 for minority spins. Our calculation of the same quantity ($\lambda_{\text{nadd}}^\sigma$) gives 0.222 for majority spins and 0.236 for minority spins. Therefore, our $\lambda_{\text{nadd}}^\uparrow$ is larger by about a factor of 3 while our $\lambda_{\text{nadd}}^\downarrow$ is larger by a factor of 1.3 than those reported in Ref. 11. Now we briefly analyze possible sources of the disagreement between our results and those reported in Ref. 11. First, we recall that $\lambda_{\text{nadd}}^\sigma$

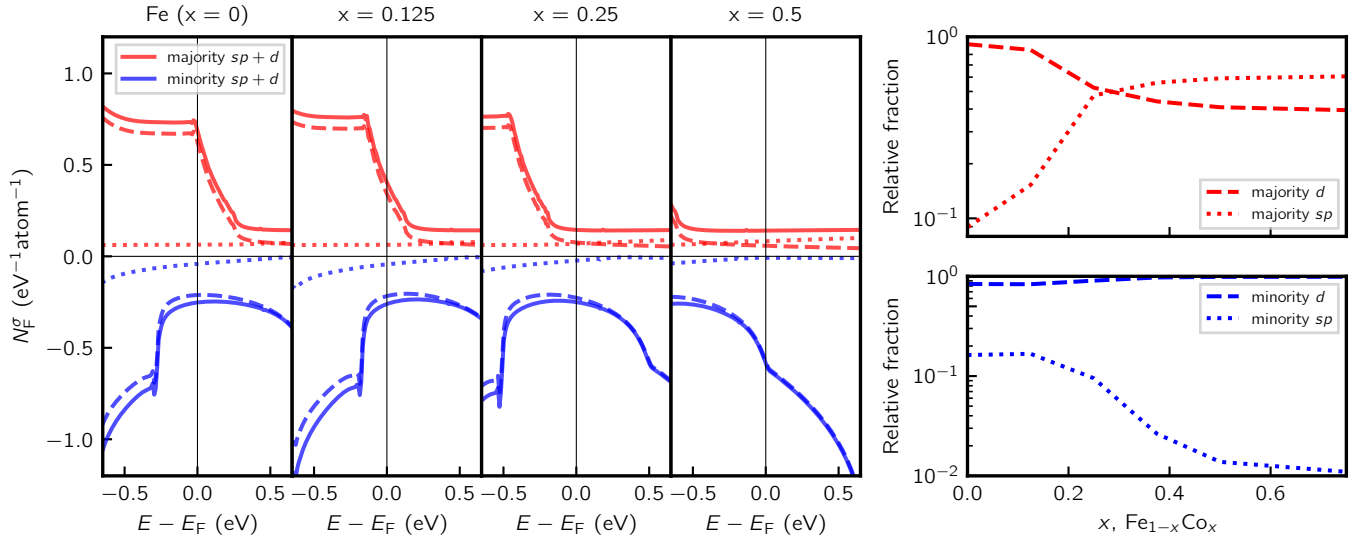


FIG. 6. Composition (x) dependence of partial density of states shows orbital character of states on majority (red lines) and minority (blue lines) Fermi surfaces. sp -like (dotted lines) to d -like (dashed lines) projections of band character are shown in the left panel and the relative fraction of the sp -like and d -like bands at the Fermi energy are shown in the right panels.

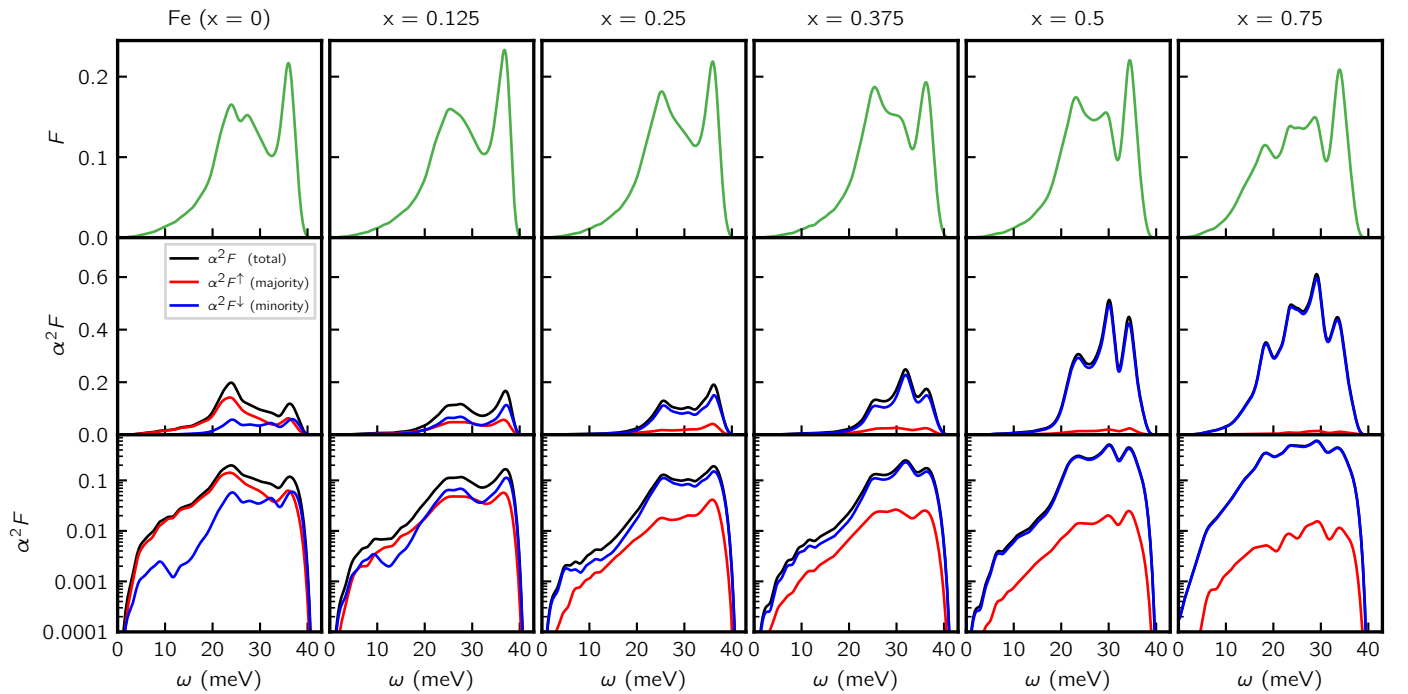


FIG. 7. Composition (x) dependence of the phonon density of states F in the upper row and the Eliashberg spectral function for total $\alpha^2 F$ (black), majority $\alpha^2 F^\uparrow$ (red) and minority $\alpha^2 F^\downarrow$ (blue) in the middle row. We show in the bottom row the $\alpha^2 F$ results on a logarithmic vertical scale.

is the product of N_F^σ and $\langle g_\sigma^2 \rangle$. Therefore, we can investigate whether the difference with respect to Ref. 11 originates from the spin-resolved density of states N_F^σ or from the average spin-resolved matrix element, $\langle g_\sigma^2 \rangle$. These quantities are given in Table. I. Comparing the

values of spin-resolved density of states we find that our N_F^\uparrow is 30% larger, while N_F^\downarrow is 25% smaller, than that reported in Ref. 11. The differences for the average matrix elements $\langle g_\sigma^2 \rangle$ are much larger. Our $\langle g_\uparrow^2 \rangle$ is nearly 2.5 times larger while $\langle g_\downarrow^2 \rangle$ about 2 times smaller. Ref. 11

reported sampling the Brillouin zone with 12^3 k points and 12^3 q points, compared to 72^3 k points and 24^3 q points that we needed to converge λ . We suspect that this difference in convergence is the main reason why the results of Ref. 11 differ from our results.

As we described previously in Sec. III B, the electron-phonon energy transfer coefficient is a physically measurable quantity closely related to λ . Several values have been reported in the literature for the electron-phonon energy transfer coefficient. A semi-empirical[37] model was used to estimate the electron-phonon energy transfer coefficient in pure Fe to be $20.8 \cdot 10^{17} \text{ W m}^{-3} \text{ K}^{-1}$, while a parameter-free model was used to obtain a value of $10.5 \cdot 10^{17} \text{ W m}^{-3} \text{ K}^{-1}$. [38]

The first-principles density functional theory was used in Ref. 41 to calculate the energy transfer coefficient as a function of the electron temperature. Extrapolation of their results to zero temperature results in an energy transfer coefficient of $7.00 \cdot 10^{17} \text{ W m}^{-3} \text{ K}^{-1}$. Using Eq. 14 we get a very similar result ($7.25 \cdot 10^{17} \text{ W m}^{-3} \text{ K}^{-1}$) for pure Fe ($x = 0$). Ref. 41 does not report G for Fe alloyed with Co. G as a function of alloy composition x are given in Table I.

We can also compare our results for G with the energy transfer coefficients obtained from the experiment. Ultrafast demagnetization measurements were used to estimate G in Fe [42] (shown in Table I) and Fe-Co alloys [9]. Ref. 9 reports a G at $x = 0$ of $33 \cdot 10^{17} \text{ W m}^{-3} \text{ K}^{-1}$ that reaches a minimum at $x = 0.25$ ($11 \cdot 10^{17} \text{ W m}^{-3} \text{ K}^{-1}$) and then increases up to $53 \cdot 10^{17} \text{ W m}^{-3} \text{ K}^{-1}$ at $x = 0.75$. Although there is a quantitative disagreement between our results and G reported in Ref. 9, there is good qualitative agreement in the composition dependence of G . From $x = 0$ to 0.25, we find a 2.7-fold decrease in G , similar to the 3.1-fold reduction found in the experiment,

and from $x = 0.25$ to 0.75, we find a 10-fold increase in G , compared to the less dramatic 5-fold increase found in the experiment.

V. CONCLUSIONS

The iron-cobalt alloy ($\text{Fe}_{1-x}\text{Co}_x$) shows strong dependence of magnetization dynamics on composition, as reported in Ref. 6 and 9. We investigated from first principles the spin-dependent strength of the electron-phonon interaction in these alloys as a function of composition (x). We find a rich dependence of the electron-phonon interaction strength λ on composition. Analyzing separately the contributions of the majority and minority spins to λ we find that both have strong, and opposing, variation with composition. Interestingly, the majority component λ^\uparrow decreases with x while the minority spin increases with x . We show that these compositional variations are driven by changes in both the density of states N_F^σ and the average elements of the electron-phonon matrix $\langle g_\sigma^2 \rangle$. The understanding of electron-phonon interaction strength in ferromagnetic alloy, such as $\text{Fe}_{1-x}\text{Co}_x$, opens doors to a better understanding of other magnetic phenomena, such as Gilbert damping,[1] ultrafast demagnetization,[2] all-optical switching,[3] and spin-dependent transport.[4, 5]

VI. ACKNOWLEDGEMENTS

This work was supported by the NSF DMR-1848074 grant.

-
- [1] T. Gilbert, A phenomenological theory of damping in ferromagnetic materials, *IEEE Transactions on Magnetics* **40**, 3443 (2004).
 - [2] E. Beaurepaire, J. C. Merle, A. Daunois, and J.-Y. Bigot, Ultrafast spin dynamics in ferromagnetic nickel, *Phys. Rev. Lett.* **76**, 4250 (1996).
 - [3] A. Kirilyuk, A. V. Kimel, and T. Rasing, Ultrafast optical manipulation of magnetic order, *Rev. Mod. Phys.* **82**, 2731 (2010).
 - [4] L. Gravier, S. Serrano-Guisan, F. Reuse, and J. P. Ansermet, Spin-dependent peltier effect of perpendicular currents in multilayered nanowires, *Phys. Rev. B* **73**, 052410 (2006).
 - [5] T. T. Heikkilä, M. Hatami, and G. E. W. Bauer, Spin heat accumulation and its relaxation in spin valves, *Phys. Rev. B* **81**, 100408(R) (2010).
 - [6] M. A. Schoen, D. Thonig, M. L. Schneider, T. Silva, H. T. Nembach, O. Eriksson, O. Karis, and J. M. Shaw, Ultra-low magnetic damping of a metallic ferromagnet, *Nature Physics* **12**, 839 (2016).
 - [7] A. J. Lee, J. T. Brangham, Y. Cheng, S. P. White, W. T. Ruane, B. D. Esser, D. W. McComb, P. C. Hammel, and F. Yang, Metallic ferromagnetic films with magnetic damping under 1.4×10^{-3} , *Nature Communications* **8**, 234 (2017).
 - [8] R. Weber, D.-S. Han, I. Boventer, S. Jaiswal, R. Lebrun, G. Jakob, and M. Kläui, Gilbert damping of CoFe-alloys, *Journal of Physics D: Applied Physics* **52**, 325001 (2019).
 - [9] R. Mohan, V. H. Ortiz, L. Vuong, S. Coh, and R. B. Wilson, Electron-phonon scattering governs both ultrafast and precessional magnetization dynamics in Co-Fe alloys, arXiv preprint arXiv:2107.11699 <https://doi.org/10.48550/arXiv.2107.11699> (2021).
 - [10] G. D. Samolyuk, L. K. Béliand, G. M. Stocks, and R. E. Stoller, Electron-phonon coupling in ni-based binary alloys with application to displacement cascade modeling, *Journal of Physics: Condensed Matter* **28**, 175501 (2016).
 - [11] M. J. Verstraete, Ab initio calculation of spin-dependent electron-phonon coupling in iron and cobalt, *Journal of Physics: Condensed Matter* **25**, 136001 (2013).

- [12] W. L. McMillan, Transition temperature of strongly-coupled superconductors, *Phys. Rev.* **167**, 331 (1968).
- [13] W. Weber, Phonon anomalies in strongly coupled superconductors, *Phys. Rev. B* **8**, 5093 (1973).
- [14] C. H. Cheng, K. P. Gupta, E. C. van Reuth, and P. A. Beck, Low-temperature specific heat of body-centered cubic Ti-V alloys, *Phys. Rev.* **126**, 2030 (1962).
- [15] E. Donato, B. Ginatempo, E. Giuliano, R. Ruggeri, and A. Stancanelli, Fermi surfaces and electron-phonon mass enhancement factor in Zr-Nb-Mo solid solutions, *Journal of Physics F: Metal Physics* **12**, 2309 (1982).
- [16] R. de Coss-Martínez, P. González-Castelazo, O. De la Peña-Seaman, R. Heid, and K. P. Bohnen, Effect of doping on lattice dynamics and electron-phonon coupling of the actinides Ac-Th alloy, *Journal of Physics: Condensed Matter* **29**, 355401 (2017).
- [17] O. DelaPena-Seaman, R. Heid, and K. P. Bohnen, Electron-phonon interaction and superconductivity in Tl-Pb-Bi alloys from first principles: Importance of spin-orbit coupling, *Phys. Rev. B* **86**, 184507 (2012).
- [18] A. Giri, M. V. Tokina, O. V. Prezhdo, and P. E. Hopkins, Electron-phonon coupling and related transport properties of metals and intermetallic alloys from first principles, *Materials Today Physics* **12**, 100175 (2020).
- [19] E. Giuliano, R. Ruggeri, E. Donato, and A. Stancanelli, Electron-phonon interaction in Nb-Mo alloys, *Nuovo Cimento B;(Italy)* **66**, <https://doi.org/10.1007/BF02725486> (1981).
- [20] M. Dacorogna, T. Jarlborg, A. Junod, M. Pelizzone, and M. Peter, Electronic structure and low-temperature properties of $V_x\text{Nb}_{1-x}\text{N}$ alloys, *Journal of low temperature physics* **57**, 629 (1984).
- [21] T. B. Massalski and U. Mizutani, Electronic band structure of hcp electron phases based on the noble metals, *Proceedings of the Royal Society of London. A. Mathematical and Physical Sciences* **351**, 423 (1976).
- [22] U. Mizutani and T. Massalski, Specific heats of alpha phase and zeta phase Ag-Al alloys in the range 1.5-4.2 k, *Journal of Physics F: Metal Physics* **5**, 2262 (1975).
- [23] F. Giustino, Electron-phonon interactions from first principles, *Rev. Mod. Phys.* **89**, 015003 (2017).
- [24] G. Eliashberg, Interactions between electrons and lattice vibrations in a superconductor, *Sov. Phys. JETP* **11**, 696 (1960).
- [25] P. B. Allen, Theory of thermal relaxation of electrons in metals, *Phys. Rev. Lett.* **59**, 1460 (1987).
- [26] P. Giannozzi, S. Baroni, N. Bonini, M. Calandra, R. Car, C. Cavazzoni, D. Ceresoli, G. L. Chiarotti, M. Cococcioni, I. Dabo, A. D. Corso, S. de Gironcoli, S. Fabris, G. Fratesi, R. Gebauer, U. Gerstmann, C. Gougoussis, A. Kokalj, M. Lazzeri, L. Martin-Samos, N. Marzari, F. Mauri, R. Mazzarello, S. Paolini, A. Pasquarello, L. Paulatto, C. Sbraccia, S. Scandolo, G. Sciauzero, A. P. Seitsonen, A. Smogunov, P. Umari, and R. M. Wentzcovitch, QUANTUM ESPRESSO: a modular and open-source software project for quantum simulations of materials, *Journal of Physics: Condensed Matter* **21**, 395502 (2009).
- [27] P. Giannozzi, O. Andreussi, T. Brumme, O. Bunau, M. B. Nardelli, M. Calandra, R. Car, C. Cavazzoni, D. Ceresoli, M. Cococcioni, N. Colonna, I. Carnimeo, A. D. Corso, S. de Gironcoli, P. Delugas, R. A. DiStasio, A. Ferretti, A. Floris, G. Fratesi, G. Fugallo, R. Gebauer, U. Gerstmann, F. Giustino, T. Gorni, J. Jia, M. Kawamura, H.-Y. Ko, A. Kokalj, E. Küçükbenli, M. Lazzeri, M. Marsili, N. Marzari, F. Mauri, N. L. Nguyen, H.-V. Nguyen, A. O. de-la Roza, L. Paulatto, S. Poncé, D. Rocca, R. Sabatini, B. Santra, M. Schlipf, A. P. Seitsonen, A. Smogunov, I. Timrov, T. Thonhauser, P. Umari, N. Vast, X. Wu, and S. Baroni, Advanced capabilities for materials modelling with QUANTUM ESPRESSO, *Journal of Physics: Condensed Matter* **29**, 465901 (2017).
- [28] D. R. Hamann, Optimized norm-conserving Vanderbilt pseudopotentials, *Phys. Rev. B* **88**, 085117 (2013).
- [29] N. Marzari and D. Vanderbilt, Maximally localized generalized Wannier functions for composite energy bands, *Phys. Rev. B* **56**, 12847 (1997).
- [30] I. Souza, N. Marzari, and D. Vanderbilt, Maximally localized Wannier functions for entangled energy bands, *Phys. Rev. B* **65**, 035109 (2001).
- [31] A. A. Mostofi, J. R. Yates, G. Pizzi, Y. S. Lee, I. Souza, D. Vanderbilt, and N. Marzari, An updated version of wannier90: A tool for obtaining maximally-localised Wannier functions, *Computer Physics Communications* **185**, 2309 (2014).
- [32] F. Giustino, M. L. Cohen, and S. G. Louie, Electron-phonon interaction using Wannier functions, *Phys. Rev. B* **76**, 165108 (2007).
- [33] S. Poncé, E. R. Margine, C. Verdi, and F. Giustino, Epw: Electron-phonon coupling, transport and superconducting properties using maximally localized Wannier functions, *Computer Physics Communications* **209**, 116 (2016).
- [34] T. Nishizawa and K. Ishida, The Co-Fe (cobalt-iron) system, *Bulletin of Alloy Phase Diagrams* **5**, 250 (1984).
- [35] M. Matsuda, K. Yamashita, R. Sago, K. Akamine, K. Takashima, and M. Nishida, Development of ductile B2-type Fe-Co based alloys, *Materials Transactions* **53**, 1826 (2012).
- [36] L. Bellaiche and D. Vanderbilt, Virtual crystal approximation revisited: Application to dielectric and piezoelectric properties of perovskites, *Phys. Rev. B* **61**, 7877 (2000).
- [37] N. Medvedev and I. Milov, Electron-phonon coupling in metals at high electronic temperatures, *Phys. Rev. B* **102**, 064302 (2020).
- [38] U. Ritzmann, P. M. Oppeneer, and P. Maldonado, Theory of out-of-equilibrium electron and phonon dynamics in metals after femtosecond laser excitation, *Phys. Rev. B* **102**, 214305 (2020).
- [39] J. P. Trinstic, Y. Wang, and H. P. Cheng, First-principles study of Co concentration and interfacial resonance states in $\text{Fe}_{1-x}\text{Co}_x$ magnetic tunnel junctions, *Phys. Rev. B* **88**, 104408 (2013).
- [40] M. Cazzaniga, L. Caramella, N. Manini, and G. Onida, Ab initio intraband contributions to the optical properties of metals, *Phys. Rev. B* **82**, 035104 (2010).
- [41] Y. V. Petrov, N. Inogamov, and K. P. Migdal, Thermal conductivity and the electron-ion heat transfer coefficient in condensed media with a strongly excited electron subsystem, *JETP letters* **97**, 20 (2013).
- [42] K. Kang and G.-M. Choi, Electron-phonon coupling parameter of ferromagnetic metal Fe and Co, *Materials* **14**, 10.3390/ma14112755 (2021).
- [43] J. J. Paggel, D.-A. Luh, T. Miller, and T. C. Chiang, Electronic-structure dependence of the electron-phonon interaction in Ag, *Phys. Rev. Lett.* **92**, 186803 (2004).
- [44] J. I. Mustafa, M. Bernardi, J. B. Neaton, and S. G. Louie, Ab initio electronic relaxation times and transport in no-

- ble metals, *Phys. Rev. B* **94**, 155105 (2016).
- [45] F. J. Pinski and W. H. Butler, Calculated electron-phonon contributions to phonon linewidths and to the electronic mass enhancement in Pd, *Phys. Rev. B* **19**, 6010 (1979).
- [46] P. B. Allen, Empirical electron-phonon λ values from resistivity of cubic metallic elements, *Phys. Rev. B* **36**, 2920 (1987).
- [47] D. A. Papaconstantopoulos, *Handbook of the band structure of elemental solids*, 2nd ed. (Springer, 2014).
- [48] T. Jarlborg and M. Peter, Electronic structure, magnetism and curie temperatures in Fe, Co and Ni, *Journal of Magnetism and Magnetic Materials* **42**, 89 (1984).